Author Contributions:
Conceptualization: Xingcai Liu, Wenfeng Liu, Hong Yang
Data curation: Xingcai Liu, Yoshihide Wada
Formal analysis: Xingcai Liu
Investigation: Xingcai Liu
Methodology: Xingcai Liu, Wenfeng Liu, Qiuhong Tang, Hong Yang
Writing – original draft: Xingcai Liu
Writing – review & editing: Xingcai Liu, Wenfeng Liu, Qiuhong Tang, Bo Liu, Yoshihide Wada, Hong Yang

Global Agricultural Water Scarcity Assessment Incorporating Blue and Green Water Availability Under Future Climate Change

Xingcai Liu[1,2,3] , Wenfeng Liu[4] , Qiuhong Tang[2,5] , Bo Liu[6], Yoshihide Wada[7] , and Hong Yang[1]

[1]Eawag, Swiss Federal Institute of Aquatic Science and Technology, Duebendorf, Switzerland, [2]Key Laboratory of Water Cycle and Related Land Surface Processes, Institute of Geographic Sciences and Natural Resources Research, Chinese Academy of Sciences, Beijing, China, [3]Key Laboratory of Compound and Chained Natural Hazards, Ministry of Emergency Management of China, Beijing, China, [4]Center for Agricultural Water Research in China, College of Water Resources and Civil Engineering, China Agricultural University, Beijing, China, [5]University of Chinese Academy of Sciences, Beijing, China, [6]International Economic & Technical Cooperation and Exchange Center, Ministry of Water Resources of China, Beijing, China, [7]International Institute for Applied Systems Analysis (IIASA), Laxenburg, Austria

Abstract Climate change was projected to have negative effects on water availability and consequently a serious constraint to food production in many areas of the world. However, such effects have not been well understood, particularly over rainfed croplands, partly because of the poor representation of green water in associated assessments. In this study, we develop an integrated agricultural water scarcity index (WSI_{ag}) that incorporates blue and green water components to examine the agricultural water scarcity in the baseline (1981–2005) and future (2026–2050) periods under the Representative Concentration Pathway (RCP)2.6 and RCP6.0 scenarios. Results show that ∼3.8 million km² (∼39% of total) croplands experienced water scarcity in the baseline period and it would expand by more than 3% in the future. Under the two scenarios, WSI_{ag} projections are similar overall and are higher than that under the baseline in 83%–84% of global total croplands. Differences are found between the scenarios in Amazonia, Southern Africa, and South Asia. The increases in future WSI_{ag} are dominated by the decreased water availability in ∼60% of total croplands and ∼24% of which is dominated by the increased crop water requirement. Changes in green water availability have a significant contribution to changes in WSI_{ag} in 16% of global croplands, mostly in arid/semiarid regions (e.g., the South edge of the Sahel, Southern Africa, Northeast China, and Central America). This implies the important role of green water management for agriculture in these regions. The integrated assessment can help develop effective strategies for agricultural water management under climate change.

Plain Language Summary Future climate change may intensify water scarcity and adversely affect crop productivity in many regions of the world. Traditionally, water scarcity assessment focused on blue water (from rivers, reservoirs, and lakes) or green water (crop evapotranspiration from soil moisture) alone. In order to examine the impact of climate change on water scarcity in croplands, we develop an integrated agricultural water scarcity index (WSI_{ag}) that incorporates blue and green water components and calculate WSI_{ag} for both historical and future periods. The assessment suggests that nearly 40% of global croplands have experienced water scarcity in the past and the situation would worsen in the future. WSI_{ag} is projected to be higher than in the past in 83%–84% of global total croplands. The increased WSI_{ag} is mostly caused by less water availability and larger crop water requirement. It is noted that changes in green water availability could also be a dominant factor in some arid/semiarid regions in the South edge of the Sahel, Southern Africa, India, Northeast China, and Central America. Our study highlights the important role of green water for agriculture water management and is expected to provide useful information for agricultural adaptation to future climate change.

1. Introduction

Water scarcity has become an increasing threat to humans and freshwater ecosystems, and the situation is expected to aggravate under future climate change (Hoekstra, 2014; Richter et al., 2020; Schewe et al., 2014; Tang, 2020). Agricultural water use is the world's largest water user and is significantly affected by climate change, socioeconomic development, and population growth (Gerten et al., 2020; Ward & Pulido-Velazquez, 2008). Intensification of agricultural water scarcity can affect food production, threatening food security, particularly to the poor (J. Huang et al., 2017; Pastor et al., 2019; Tong et al., 2016; Yin et al., 2017). On the other hand, increased water

use in economic sectors can deleteriously affect freshwater ecosystems (Dudgeon, 2010; Richter et al., 2020), as well as the fulfillment of environmental flow requirement (EFR) for maintaining healthy river ecosystems. This, in turn, might further aggregate agricultural water scarcity and impair the sustainability of food production in the future (Jägermeyr et al., 2017). Understanding agricultural water scarcity under climate change is therefore important given the increasing food demands and consequently intensified irrigation and expansion of cropland in the future (FAO, 2018).

Most previous studies on water scarcity have focused solely on blue water withdrawal/use and blue water availability (i.e., water from rivers, reservoirs, and lakes). They generally reported that future water scarcity would further aggregate over many regions of the world (W. Liu et al., 2019; X. Liu et al., 2019; Schewe et al., 2014). However, assessments based on blue water only may not fully reflect the actual water stress conditions of crop productions (Núñez et al., 2013; Quinteiro et al., 2018). This is because green water (i.e., water can be evaporated by crops from rainwater or soil moisture) is the sole water source for rainfed cultivations and an important part of the water source for irrigated croplands. Thus, changes in green and blue water availability and consumption will influence agricultural water scarcity (J. Liu et al., 2017; X. Liu et al., 2017; Veettil & Mishra, 2016). Furthermore, agriculture is the largest water user and would be prone to conflict with increasing water demands from other users in the future. This makes it more sensitive to climate change in many regions, and it is necessary to have a systematic assessment of the status of agricultural water scarcity and projection of its future changes (Gerten et al., 2011; Rosa et al., 2020). Such assessments can be instrumental in understanding the dependence between human water use, agricultural water demands, and EFR, which reflects the linkages between the sustainable development goal (SDG) 6 (clean water and sanitation), SDG 2 (zero hungry), and the SDG 15 (life on land).

Recently, some efforts have been made to improve the representation of water scarcity with different types of definitions concerning water use and availability. Hoekstra et al. (2012) examined water scarcity using the concept of water footprint. They used blue water footprint, which is defined as consumptive use of ground- and surface water flows. They also accounted for the environmental flows needed to sustain critical ecological functions by considering monthly values for major river basins across the world. Rodrigues et al. (2014) suggested that blue water scarcity index and green water scarcity index may indicate distinct temporal patterns of water scarcity. Schyns et al. (2019) examined green water scarcity using green water footprint and pointed out that growing green water scarcity would pose a considerable threat to natural ecosystems. Quinteiro et al. (2019) mapped green water scarcity under climate change in Portugal and emphasized the importance of the management of green water for ensuring high crop productivity. Veettil and Mishra (2020) used two indices of water use to water availability, that is, green water scarcity index and blue water scarcity index, to assess the overall water security at the county level of the Contiguous United States. Based on the concept of water footprint, Rosa et al. (2020) introduced an economic agricultural water scarcity index (WSI_{ag}) for the croplands, defined as lack of irrigation due to limited institutional and economic capacity instead of hydrologic constraints. They developed a monthly agro-hydrological analysis to map agricultural regions affected by agricultural economic water scarcity, which accounts for up to 25% of the global croplands. W. Liu et al. (2022) developed an integrated index that includes both blue and green water availability to assess agricultural water scarcity. They validated the proposed index by comparing it with traditional water scarcity index during the historical period (1971–2010). So far, studies that have explicitly incorporated both green water and blue water components in one integrated index for global water scarcity assessment under future climate change are generally absent. Such an assessment based on a comprehensive depiction of agricultural water scarcity would provide a better understanding of the potential impact of future climate change on food production.

To address the above research gap, we proposed an WSI_{ag} that incorporates blue water and green water use and availability as well as EFR to assess current and projected future changes in agricultural water scarcity. It was designed to indicate the extent to which water availability could not meet agricultural water demands. Global agricultural water scarcity conditions were assessed for the baseline period (1981–2005) and the future period (2026–2050) considering two climate change scenarios. As many as 19 major crops, which account for ~80% of global total croplands, were considered in the assessment. The explicit inclusion of green water and EFR enables the comprehensive assessment of agriculture water scarcity for both irrigated and rainfed croplands. A better understanding of agricultural water scarcity can support the development of measures for integrated water resource management for humans and nature under future climate change.

2. Materials and Methods

2.1. Agricultural Water Scarcity Index

In this study, the WSI_{ag} was defined as a ratio of water demand to water availability in crop production taking into consideration of blue water, green water, and EFR following W. Liu et al. (2022). It measures the extent to which the sum of green water and blue water availability can meet the crop water requirements and is estimated by the following equation:

$$\text{WSI}_{ag} = \frac{\text{ET}_c}{\text{WA}} \tag{1}$$

$$\text{WA} = \text{IE} \times \text{WA}_{blue} + \text{WA}_{green} \tag{2}$$

where ET_c is total water requirements of the 19 crops (m³/month), IE is irrigation efficiency, WA_{blue} is agricultural blue water availability (m³/month), and WA_{green} is agricultural green water availability (m³/month). The IE is a combination of three partial efficiencies, that is, conveyance efficiency, field efficiency, and distribution efficiency, of which the last one was represented by a management factor (Rohwer et al., 2007). The map of national level IE with a spatial resolution of $0.5° \times 0.5°$ (see Figure S1a in Supporting Information S1) was derived from Rohwer et al. (2007).

Agricultural blue water availability is estimated by the following equation:

$$\text{WA}_{blue} = Q - \text{WW}_{noag} - \text{EFR} \tag{3}$$

where Q is the total blue water resources (m³/month) determined by natural streamflow, WW_{noag} is water withdrawal (m³/month) for nonagricultural (i.e., industrial and domestic) sectors, and EFR is environmental flow requirements (m³/month). EFR is estimated by using the Variable Monthly Flow (VMF) method under a "fair" ecological condition globally (Pastor et al., 2014; see Table S1 in Supporting Information S1). This enables consideration of temporal and spatial variations of EFR across different river systems globally. WA_{blue} is estimated over the whole individual grid cells having croplands.

In this study, agricultural green water availability was estimated as the water evaporated by crops from rainwater or soil moisture (m³/month) over croplands of individual grid cells, which was computed by the PCR-GLOBWB model (Wada et al., 2014). In the PCR-GLOBWB model, crop evapotranspiration from rainwater and irrigation (blue water) was calculated separately for the irrigated croplands. The simulated actual transpiration under nonirrigated conditions was estimated as green water availability (Wada et al., 2011). It should be noted that the WA_{green} might be underestimated in the case that crops do not deplete the intercepted rainwater and available soil moisture in the root zone.

WSI_{ag} was calculated on a monthly basis and averaged over the entire period for the analysis of their spatial patterns or averaged for each month for regions for hot spot analysis. To be in line with previous studies (Hanasaki et al., 2018; Hoekstra et al., 2012; Oki & Kanae, 2006; Vörösmarty et al., 2000), the conventional threshold of 0.4 ($\text{WSI}_{ag} > 0.4$), that is, the volume of ET_c exceeds 40% of total water availability, is used to identify agricultural water scarcity. It should be noted that the threshold of 0.4 may not consistently reflect the status of water scarcity across regions due to different proportions of return flow of water withdrawal to water bodies (J. Liu et al., 2017).

2.2. Crop Water Requirements

Water requirements of crops (ET_c) over both rainfed and irrigated croplands were estimated as the evapotranspiration under standard conditions where no limitations are placed on crop growth or evapotranspiration with the modified Penman–Monteith method described in the FAO-56 report (Allen et al., 1998). Cropland area, crop planting, and harvest date of the 19 crops (see Table S2 and Figure S1b in Supporting Information S1) were derived from the MIRCA2000 data (Portmann et al., 2010). ET_c was calculated based on daily data and then aggregated for each month. Specifically, ET_c^* was determined by applying the dual crop coefficient approach based on the reference evapotranspiration (ET_0). ET_0 was estimated by the Penman–Monteith method (Allen et al., 1998):

$$\mathrm{ET}_0 = \frac{0.408\Delta(R_{\mathrm{n}} - G) + \gamma \frac{900}{T+273} u_2(e_{\mathrm{s}} - e_{\mathrm{a}})}{\Delta + \gamma(1 + 0.34u_2)} \tag{4}$$

where Δ is slope vapor pressure curve (kPa °C^{-1}), R_{n} is net radiation at the crop surface (MJ m^{-2} day^{-1}), G is soil heat flux density (MJ m^{-2} day^{-1}), T is mean daily air temperature at 2 m height (°C), u_2 is wind speed at 2 m height (m s^{-1}), e_{s} is saturation vapor pressure (kPa), e_{a} is actual vapor pressure (kPa), and γ is psychrometric constant (kPa °C^{-1}).

For each crop, ET_{c} was then calculated by the following equation:

$$\mathrm{ET}_{\mathrm{c}} = (K_{\mathrm{cb}} + K_{\mathrm{e}}) \times \mathrm{ET}_0 \tag{5}$$

where K_{cb} is the basal crop coefficient for the individual crops and K_{e} is the coefficient for soil evaporation.

K_{cb} was often determined based on the recommended values according to the climate conditions for different growing stages of each crop using the following equation:

$$K_{\mathrm{cb}} = K_{\mathrm{cb}}^* + (0.04(u_2 - 2) - 0.004(\mathrm{RH}_{\min} - 45)) \times \left(\frac{h}{3}\right)^{0.3} \tag{6}$$

where K_{cb}^* is the recommended values under subhumid climate (relative humidity = 45%) and moderate wind speed (2 m s^{-1}) for each growing stage (Table S2 in Supporting Information S1); $\mathrm{RH}_{\min}$ is minimum relative humidity (%); h is crop height (m) and it reaches the maximum height of crops during the mature stage. Before the mature stage, h was determined as the proportion of the maximum crop height according to the difference between the current date and mature stage.

The coefficient for soil evaporation K_{e} was estimated as follows:

$$K_{\mathrm{e}} = \min(K_{\mathrm{r}} \times (K_{\mathrm{c,max}} - K_{\mathrm{cb}}), \, f_{\mathrm{ew}} \times K_{\mathrm{c,max}}) \tag{7}$$

where K_{r} is dimensionless evaporation reduction coefficient dependent on the cumulative depth of water depleted from the topsoil; f_{ew} is the fraction of the soil that is both exposed and wetted; $K_{\mathrm{c,max}}$ is the maximum value of K_{cb} and can be estimated by the following equation:

$$K_{\mathrm{c,max}} = \max\left(\left(1.2 + (0.04(u_2 - 2) - 0.004(\mathrm{RH}_{\min} - 45)) \times \left(\frac{h}{3}\right)^{0.3}\right), \, K_{\mathrm{cb}} + 0.05\right) \tag{8}$$

f_{ew} was calculated as

$$f_{\mathrm{ew}} = \min(1 - f_{\mathrm{c}}, \, f_{\mathrm{w}}) \tag{9}$$

where f_{c} is the average fraction of soil surface covered by vegetation, f_{w} is the average fraction of soil surface wetted by irrigation or precipitation and has a minimum value of 0.01 (for irrigated croplands or no rainfall conditions). For rainfed cropland, f_{w} is 1 if precipitation rate is larger than 5 mm day^{-1}. f_{c} can be estimated using the relationship:

$$f_{\mathrm{c}} = \left(\frac{K_{\mathrm{cb}} + K_{\mathrm{c,min}}}{K_{\mathrm{c,max}} - K_{\mathrm{c,min}}}\right)^{1+0.5h} \tag{10}$$

where $K_{\mathrm{c,min}}$ is the minimum K_{c} for dry bare soil with no ground cover (0.15 was used in this study).

2.3. Analysis and Attribution of the Changes in WSI$_{\mathrm{ag}}$

Monthly WSI$_{\mathrm{ag}}$ was calculated based on the simulations of water availability, water withdrawal, and ET$_{\mathrm{c}}$ for the baseline (1981–2005) and future (2026–2050) periods. Multiyear means of these monthly variables were calculated at the grid cell level for spatial analysis. Regional analysis was conducted based on the spatial aggregation of the mean monthly WSI$_{\mathrm{ag}}$. Future projections of WSI$_{\mathrm{ag}}$ were adjusted by removing the systematic biases between the historical simulations driven by GCM data and observation-based forcing data. Mean values across the three

observation-based meteorological forcings were used, and the mean values of future projections across the four GCMs were used for the main analysis.

Future changes in WSI$_{ag}$ can be attributed to the changes in ET$_c$ and WA (green and blue) with the differential of Equation 1:

$$\Delta WSI_{ag} = \frac{dWSI_{ag}}{dET_c}\Delta ET_c + \frac{dWSI_{ag}}{dWA}\Delta WA = \frac{1}{WA}\Delta ET_c - \frac{ET_c}{WA^2}\Delta WA \qquad (11)$$

$$\Delta WA = \Delta WA_{blue} + \Delta WA_{green} \qquad (12)$$

where ET$_c$ and WA are the mean values for the baseline period; Δ indicates the future changes compared to the baseline period. The larger item on the right side in Equation 11 would be viewed as the dominant factor on ΔWSI_{ag}; if the dominant factor is ΔWA, the dominant factor of ΔWA would be further determined by the larger item on the right side in Equation 12.

2.4. Data Source

Three observation-based global meteorological data sets, namely PGMFD v.2 (Sheffield et al., 2006), GSWP3 (http://hydro.iis.u-tokyo.ac.jp/GSWP3/), and WFDEI (Weedon et al., 2014), were used to calculate ET$_c$ over the baseline period. These data sets were obtained from the Inter-Sectoral Impact Model Intercomparison Project phase 2a (ISIMIP2a). The bias-corrected climate projections of four GCMs (namely GFDL-ESM2M, HadG-EM2-ES, IPSL-CM5A-LR, and MIROC5) provided by the ISIMIP phase 2b (ISIMIP2b; Frieler et al., 2017) were used to calculate the ET$_c$ over the future period (see Table S3 in Supporting Information S1 for more details).

Global hydrological simulations with spatial resolutions of $0.5° \times 0.5°$ by the PCR-GLOBWB model (Wada et al., 2014, 2016) from ISIMIP2a and ISIMIP2b archives were used for the analysis of baseline and future periods, respectively. The baseline simulations were based on the three meteorological forcing data sets following the ISIMIP2a protocol, and the four GCMs were used to drive the PCR-GLOBWB model for both historical and future periods following the ISIMIP2b protocol (Frieler et al., 2017). Two Representative Concentration Pathways (RCPs), namely the low-emission scenario RCP2.6 and the no-mitigation scenario RCP6.0, were considered for future projections as per the ISIMIP2b protocol. Under the RCP6.0, the emissions of greenhouse gases will peak around 2060, which could be a good reference for the goal of UN Climate Change Conference 2021 global net zero by the middle of the century (https://ukcop26.org/cop26-goals).

In this study, we used the simulations of monthly streamflow (the variable "dis" in the ISIMIP archive) to estimate blue water availability. The simulations of green water use (the variable "airrusegreen" for irrigated croplands and "arainfusegreen" for rainfed croplands) were used to estimate green water availability. Simulations of monthly water withdrawal for irrigation, industrial (including electricity and manufacturing water use), and domestic (including municipal and public) sectors were used to calculate the blue water availability in combination with the streamflow. The combined data set based on HYDE (Goldewijk et al., 2017) and MIRCA (Portmann et al., 2010) was used to derived the rainfed and irrigated croplands during the historical period in the PCR-GLOBWB model. The socioeconomic conditions (e.g., population, gross domestic production, and land use) of the year 2005 were used for the simulations of future water withdrawals. Hence, in this study, the trajectory of the future socioeconomic conditions was not considered in the agricultural water scarcity assessment.

3. Results

3.1. Baseline Agricultural Water Scarcity

The spatial patterns of WA$_{blue}$ (Figure 1a) and WA$_{green}$ (Figure 1b) were generally different because the former was particularly high along the rivers while the latter was often high in the regions with dense croplands (Figure S1b in Supporting Information S1). The spatial patterns of ET$_c$ (Figure 1c) resemble the distribution of croplands. High WSI$_{ag}$ values were found in the regions with intensive croplands and some arid regions (Figure 1d). The distribution of WSI$_{ag}$ differs somewhat from the conventional WSI in the previous studies (e.g., Oki & Kanae, 2006; Wada et al., 2011) because of the different structure of the calculation formula. We focused on assessing water scarcity in agriculture, that is, crop ET$_c$ was used in this study while water withdrawal in all
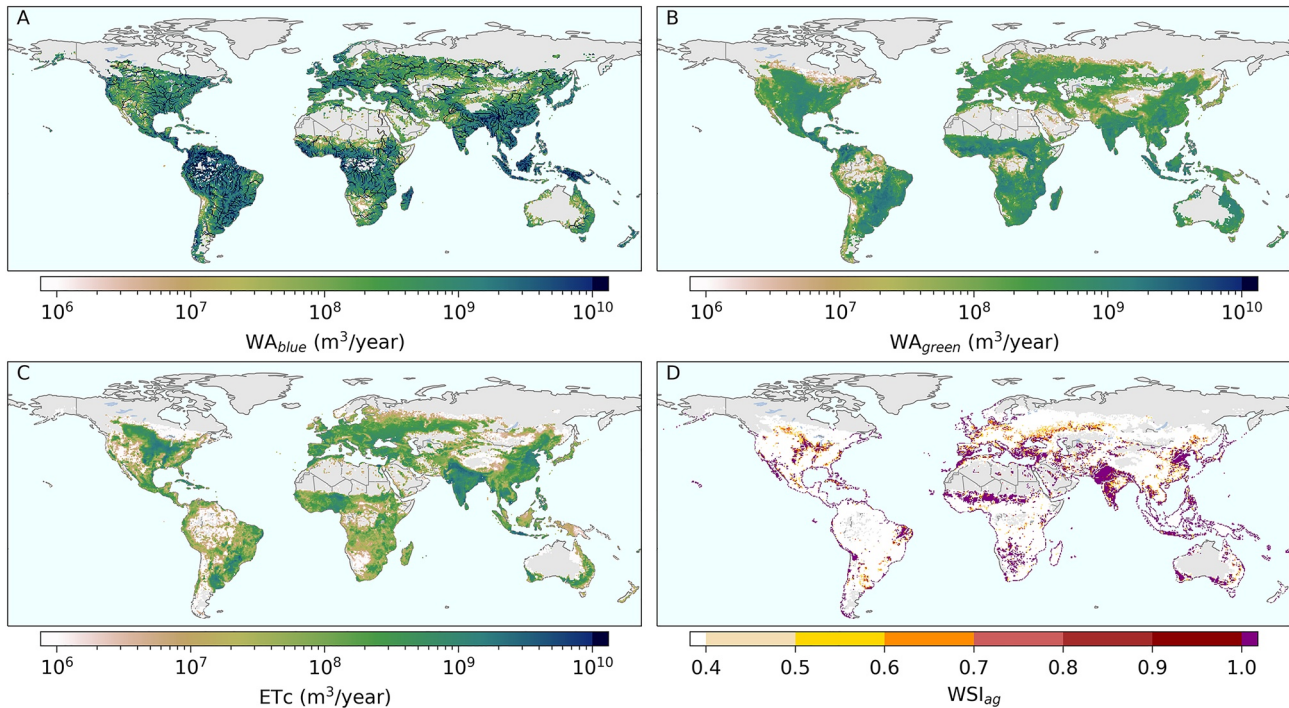
Figure 1. Water availability and agricultural water requirements (ET$_c$) during the baseline period (1981–2005) at grid cell (0.5° × 0.5°) level. (a) Blue water availability (WA$_{blue}$), (b) green water availability (WA$_{green}$), (c) crop water requirement (ET$_c$), and (d) agricultural water scarcity index (WSI$_{ag}$).

sectors was considered in the previous studies as the numerator. There were about 3.8 million km^2 (39% of the global total) croplands under water scarcity over the world during the baseline period.

3.2. Future Changes in Crop Water Requirements and Water Availability

The ET$_c$ was projected to increase over ~90% of croplands of the world during 2026–2050 under both RCP2.6 and RCP6.0 compared to the baseline period (Figures 2a and 2b). The relative increase in ET$_c$ was particularly large in Europe and Eastern United States, which was corresponding to the large increases in temperature in these regions (Figure S2 in Supporting Information S1). Slight differences between the two scenarios were found in Southern Africa and East Asia where ET$_c$ shows larger increases under RCP2.6 than RCP6.0. This is very likely associated with the different increments in future temperature in these regions (see Figures S2a and 2b in Supporting Information S1). Globally, ET$_c$ would increase by 3.4% and 2.89% under RCP2.6 and RCP6.0, respectively (Table S4 in Supporting Information S1).

In contrast, changes in WA showed large spatial variability over the world (Figures 2c and 2d). Relatively large increases in WA were found in the South of Sahel, India, Western Russia, and Northern China, while large decreases were found in Amazonia, Northern Europe, Central and Eastern US, and Central and Southern Africa. Larger increases (decreases) were found in the South of Sahel and India (Amazonia and Central and Southern Africa) under RCP2.6 than that under RCP6.0. At the global level, the total WA would decrease slightly under RCP2.6 (−0.86%) and RCP6.0 (−0.17%; Table S4 in Supporting Information S1).

The relative changes in blue water availability (WA$_{blue}$) showed evident uneven spatial distributions (Figures 2e and 2f) under both scenarios. For RCP2.6, WA$_{blue}$ would decrease in Central and Eastern North America, Northern and Eastern Europe, large parts of South America, Central and Southern Africa, and Australia. WA$_{blue}$ showed similar spatial patterns under RCP6.0, but with fewer decreases in South America, Europe, and Africa but larger decreases in North America compared to RCP2.6. The increases in WA$_{blue}$ were also smaller under RCP6.0 than RCP2.6. The relative changes in green water availability (WA$_{green}$, Figures 2g and 2h) were much different from WA$_{blue}$, characterized by opposite changes in some regions, for example, the Western US, some parts of South America, Central Africa, and Southeast Asia. Large decreases in WA$_{green}$ were found in the high latitudes
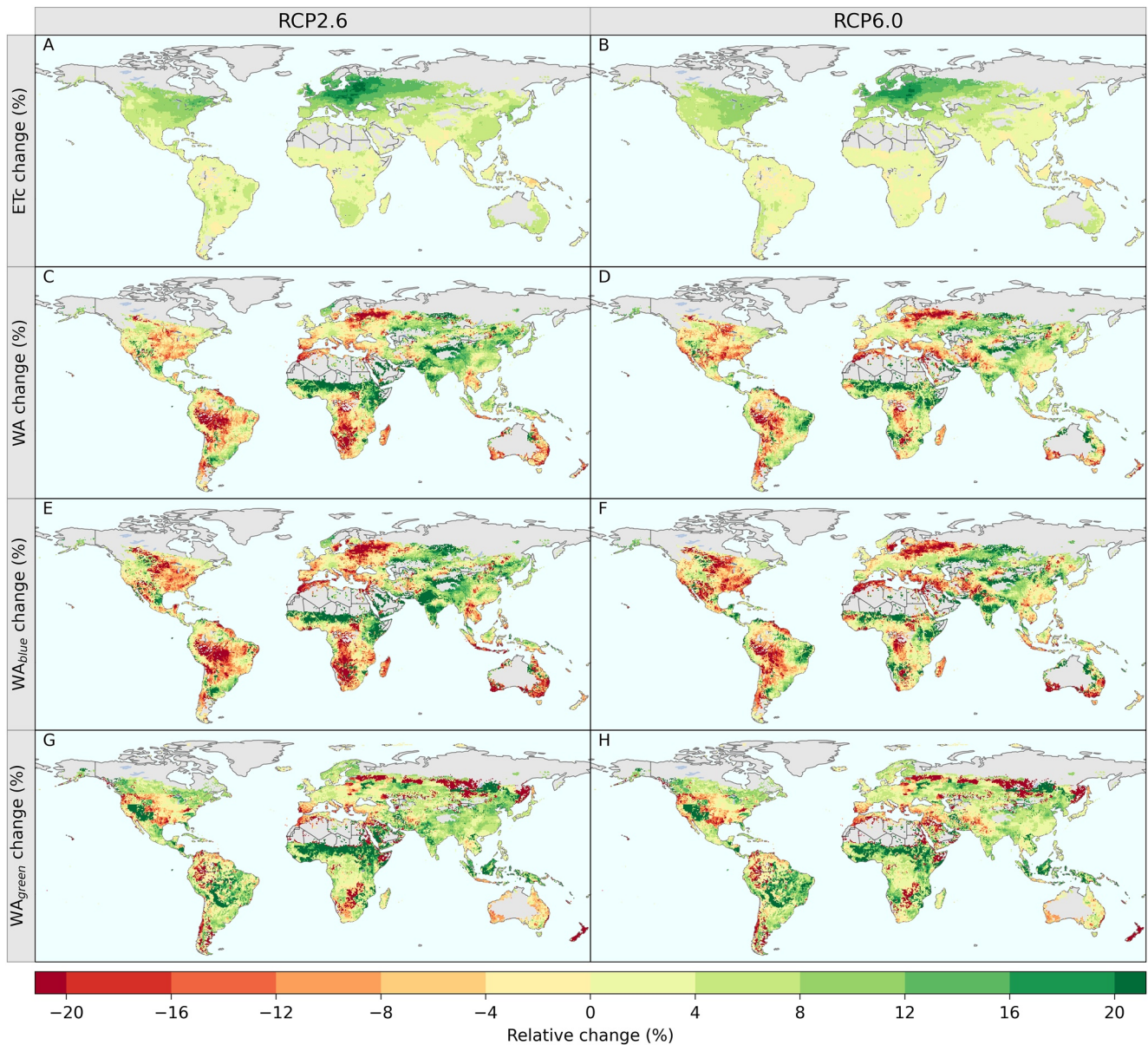
Figure 2. Changes in agriculture water requirements (ET$_c$) and water availability (WA) in the future (2026–2050) for RCP2.6 and RCP6.0. WA$_{blue}$, blue water availability; WA$_{green}$, green water availability. (a, c, e, and g) Changes in ET$_c$, WA, WA$_{blue}$, and WA$_{green}$ for RCP2.6, respectively. (b, d, f, and h) Changes in ET$_c$, WA, WA$_{blue}$, and WA$_{green}$ for RCP6.0, respectively.

of Eurasia. It is noticeable that at the global level, the decrease in WA was mainly due to the decline in WA$_{blue}$, WA$_{green}$ was projected to increase by 3.66% and 3.26% under RCP2.6 and RCP 6.0, respectively (Table S4 in Supporting Information S1).

The different patterns in the changes in ET$_c$ and WA (especially WA$_{blue}$) between the two scenarios could be largely associated with the different changes in future temperature and precipitation (Figure S2 in Supporting Information S1), respectively. Specifically, the changes in ET$_c$ would be associated with the larger increases in temperature in the high latitudes of Eurasia and Eastern North America, while the changes in WA would be associated with the larger increase in precipitation over the South of Sahel, India, and East Asia under RCP2.6 than RCP6.0 (Figure S2 in Supporting Information S1).
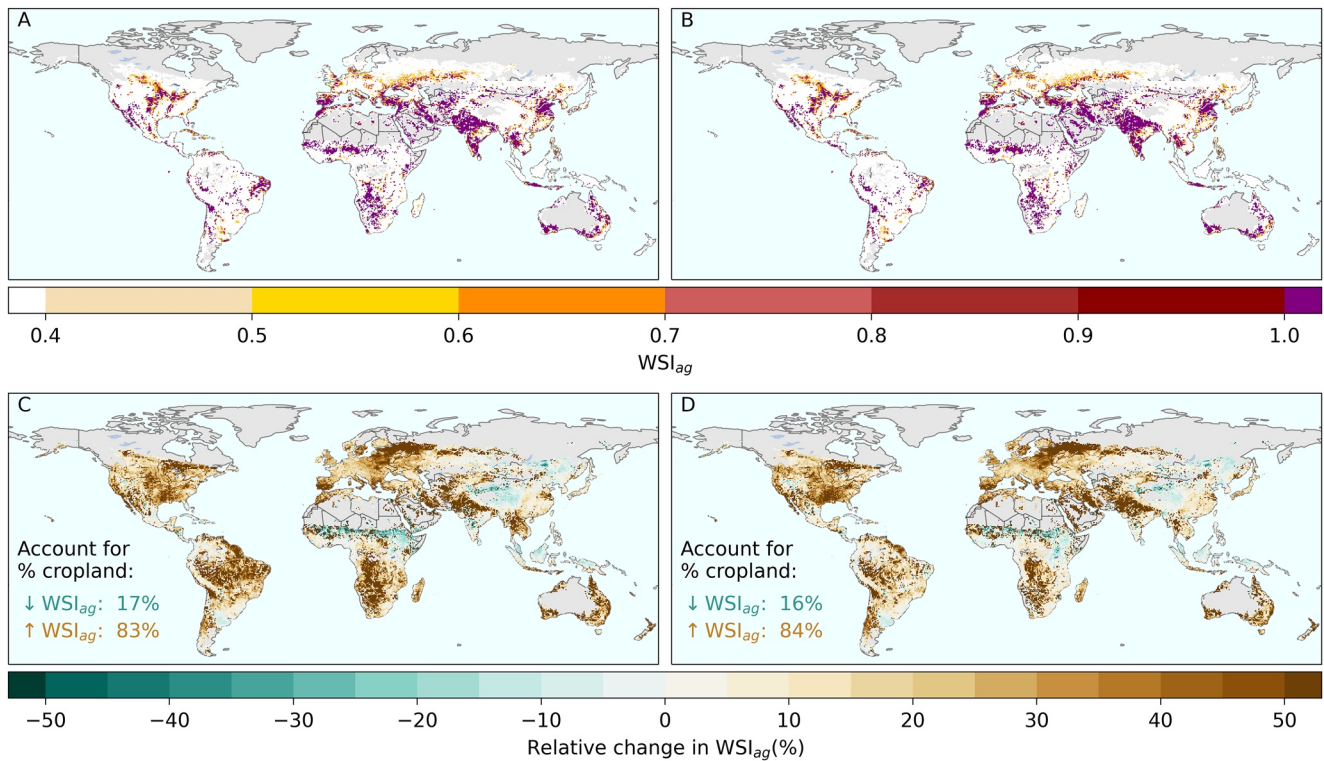
Figure 3. Mean agricultural water scarcity index (WSI_{ag}) during 2026–2050. Mean WSI_{ag} for RCP2.6 (a) and RCP6.0 (b), and relative changes (%) in WSI_{ag} compared to the baseline period (1981–2005) for RCP2.6 (c) and RCP6.0 (d). The percentages in (c) and (d) are the proportions of total cropland area showing decreased (↓) or increased (↑) WSI_{ag}.

3.3. Future Changes in Agricultural Water Scarcity

For both scenarios, future WSI_{ag} (Figures 3a and 3b) would become larger compared to the baseline period by showing values greater than 0.4 in many regions with dense croplands, for example, Central United States, North India, and North China as well as some arid regions like North Africa and Central Asia. WSI_{ag} would increase in 83%–84% of total croplands and decrease in only 16%–17% of the croplands in the future (Figures 3c and 3d). Large relative changes in WSI_{ag} were found in Central and Eastern United States, Amazonia, Northern Eurasia, Southern Africa, North India, and parts of Central Asia. The spatial patterns were generally similar for the two scenarios. However, there are significant regional differences. It is noticeable that the relative changes are smaller under RCP6.0 than that under RCP2.6 in some regions, for example, Southeast Asia, Amazonia, and Southern Africa, and the opposite was found in South Asia and Central Asia.

3.4. Cropland Areas Affected by WSI and Their Changes in the Future

The cropland under water scarcity (A_{ws}) and future changes were estimated for the top 10 countries with the largest croplands (see Table S5 in Supporting Information S1 for all countries), continents, and the globe (Table 1). During the baseline period, about 3.8 million km^2 croplands suffered water scarcity, which accounts for ~39% of global total croplands. A_{ws} ranges from 73 to 760 thousand km^2 across the 10 countries. A_{ws} was the largest in India (760 thousand km^2, 49% of total croplands) and was the second-largest in China (730 thousand km^2, 52% of total croplands). The third-largest A_{ws} was in the United States (479 thousand km^2, 47% of total croplands). A_{ws} was the smallest in Pakistan (73 thousand km^2, 36% of the regional croplands). The A_{ws} (117 thousand km^2) accounted for the largest proportion (~57%) of croplands in Australia and the smallest proportion (22%) in Brazil. The A_{ws} was nearly one third of total croplands in Russia, Nigeria, Argentina, and Canada. For the continents, A_{ws} was the largest in East Asia and Pacific (1,110 thousand km^2, ~50% of total croplands), followed by the A_{ws} in South Asia (905 thousand km^2, 46% of total croplands) and was the smallest in North Africa and Central

Table 1
Crop Area Under Water Scarcity (A_{ws}) During the Baseline (1981–2005) and Future (2026–2050) Periods for Countries, Continents, and the Globe

Country	Baseline A_{ws} (10^3 km²)	Baseline A_{ws} (% cropland)	RCP2.6 ΔA_{ws} (%)	RCP6.0 ΔA_{ws} (%)
India	760	48.79	1.86	4.76
China	730	51.8	0.8	0.61
United States	479	47.16	**3.96**	**4.06**
Brazil	94	22.03	**10.77**	3.38
Russia	127	27.17	**9.28**	**7.93**
Nigeria	89	33.18	−4.26	−3.22
Argentina	85	33.92	−3.42	−2.35
Canada	77	31.47	2.17	2.71
Australia	117	56.67	**5.94**	**5.24**
Pakistan	73	36.3	15.74	21.37
Continent				
East Asia and Pacific	1,110	49.32	1.83	1.21
South Asia	905	46.36	2.80	5.61
Europe	613	32.48	**7.32**	**6.56**
North America	556	44.12	3.71	**3.87**
Sub-Saharan Africa	263	24.48	−2.43	−2.48
Latin and South America	251	25.31	**3.89**	1.98
North Africa and Central Asia	101	33.81	**5.78**	**8.51**
Global	3,800	39.11	**3.03**	**3.27**

Note. Absolute A_{ws} and the proportions of croplands of each region in the baseline were shown in the first and second columns, respectively. The changes in A_{ws} (ΔA_{ws}) in the future period compared to the baseline period under RCP2.6 and RCP6.0 are shown in the third and fourth columns, respectively. Bold numbers indicate high agreements (the same direction of change) in ΔA_{ws} across the four GCMs.

Asia (101 thousand km², one third of total croplands). The A_{ws} accounted for nearly one third of total croplands in Europe (613 thousand km²) and 44% of total croplands in North America (556 thousand km²). A_{ws} was more than 250 thousand km², accounting for about one quarter of total croplands, in Sub-Saharan Africa and Latin and South America.

Global A_{ws} would increase by more than 3% in the future under both scenarios compared to the baseline period. Future changes in A_{ws} (ΔA_{ws}) vary across the 10 countries, ranging from −4.26% to 15.74% for RCP2.6 and from −3.22% to 21.37% for RCP6.0. The largest relative change in A_{ws} was found in Pakistan (15.74% and 21.37%), followed by Brazil (10.77% and 3.38%) and Russia (9.28% and 7.93%). A_{ws} would increase by more than 5% in Australia and 1.86%–4.76% in India. Increases of 2.17%–2.71% in A_{ws} were found in Canada and less than 1% is found in China. A_{ws} would decrease by 4.26%–3.22% in Nigeria and by 3.42%–2.35% in Argentina. At the continental scale, the increases in A_{ws} were large in North Africa and Central Asia (5.78% and 8.51%) and Europe (7.32% and 6.56%), followed by North America (3.71% and 3.87%). The smallest increases in A_{ws} were found in East Asia and the Pacific (1.83% and 1.21%), while decreases were found in Sub-Saharan Africa (2.43% and 2.48%).

Despite large uncertainties between the four GCMs (see Table S5 in Supporting Information S1), the ΔA_{ws} showed general agreements (the same direction of change) across the four GCMs under both scenarios for the globe, Europe, North Africa, and Central Asia, United States, Russia, and Australia. High agreements in ΔA_{ws} were also found in Brazil and Latin and South America under RCP2.6 and in North America under RCP6.0.
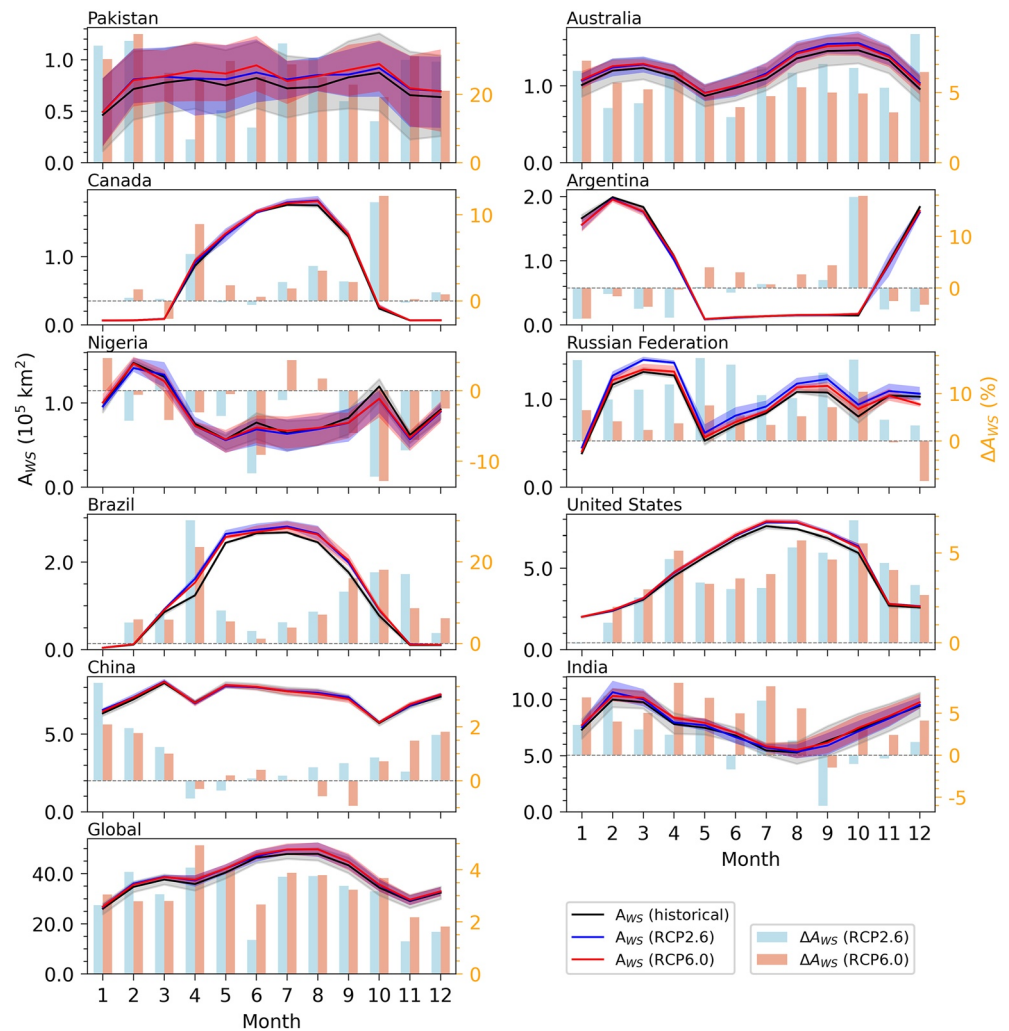
Figure 4. Crop area under water scarcity (A_{ws}) in the future (2026–2050) and the relative changes of A_{ws} (ΔA_{ws}) compared to the baseline period (1981–2005). The shadow areas show the maximum and minimum A_{ws} of each month across the four GCMs.

The impact of water scarcity on agricultural production is strongly associated with its occurrence in a year. The average monthly water scarcity situation during the 2026–2050 period was examined at the country level, as well as the global scale. A_{ws} for each month over the future period showed distinct patterns between the 10 countries having large croplands and the globe (Figure 4). Generally, A_{ws} is large (more than 4 million km^2) during the growing season (April–October) and relatively small in other months for the globe. The same pattern was found in Canada, Russia, and the United States and the almost opposite pattern of A_{ws} was found in Argentina. The variations in A_{ws} are relatively small in Pakistan and China. In some southern countries like Australia and Brazil, A_{ws} showed roughly two peaks and was relatively small in May. A_{ws} is small in summer and large in winter and spring in India, as well as in Nigeria. For India and China which have large croplands, A_{ws} is larger than 0.5 million km^2 for each month for both baseline and future periods. For the United States which has the third-largest croplands, A_{ws} is larger than 0.2 million km^2 in all months and reach 0.8 million km^2 in summer months. The spread between GCMs is significant in the A_{ws} of Pakistan, Australia, and Nigeria.

Overall, global A_{ws} would increase in all months by nearly 1%–4% in the future. Increases were found in almost all months in the eight countries excluding Argentina and Nigeria. A_{ws} would decrease in Nigeria for most months and Argentina for winter and spring. In China, ΔA_{ws} is larger in winter and spring and small or negative in other months. Large increases were found in Pakistan (~20% under RCP6.0) and Russia (~20% in April and October).
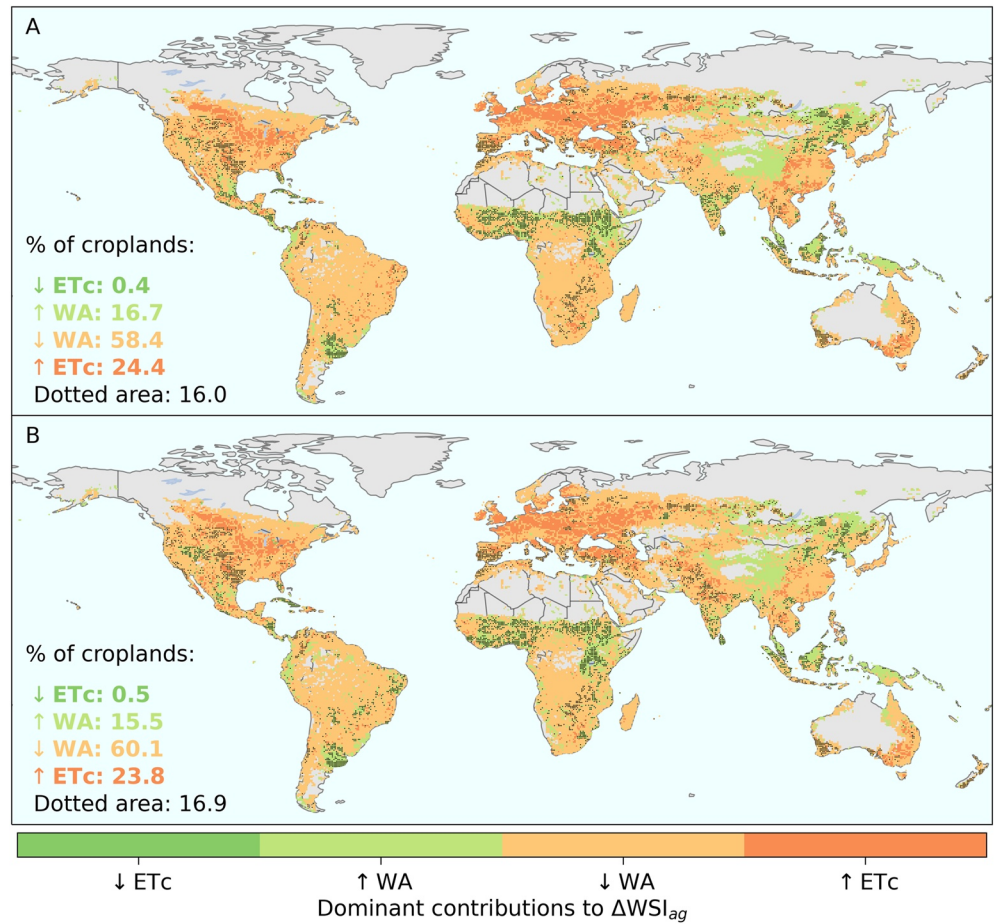
Figure 5. Dominant contributions to changes in agricultural water scarcity (ΔWSI_{ag}) and water availability (ΔWA) under RCP2.6 (a) and RCP6.0 (b). Green colors indicate decreases in WSI_{ag}, and orange colors indicate increases in WSI_{ag}. ↑ and ↓ indicate increases and decreases, respectively, in ET_c or WA. The dotted area indicates the ΔWA is dominated by changes in green water availability (WA_{green}). The colored numbers in the plots indicate the proportions of total cropland area for individual contributing factors, for example, "↓ET_c: 0.4" means "decreased ET_c dominates the decreased WSI_{ag} in 0.4% of global croplands.".

3.5. Contributions of Changes in ET_c and WA to WSI_{ag}

Changes in future WSI_{ag} can be attributed to changes in ET_c and WA. We identified the dominant contributor to changes in WSI_{ag} across the world croplands for the period 2026–2050 under the two RCPs (Figure 5). It was found that the changes in WA would be the dominant contributions to the changes in WSI_{ag} (ΔWSI_{ag}) in ∼75% of global total croplands. Specifically, the increases (decreases) in WSI_{ag} will be dominated by the decreases (increases) in WA in ∼60% (∼16%) of total croplands. The decreases in WSI_{ag} dominated by the increases in WA are mostly found in arid regions like the Tibetan Plateau and its surrounding areas, and the South of Sahel, and some humid regions like Southern South America and Southeast islands, while the decreasing WA lead to larger WSI_{ag} across the world.

The increases in ET_c would result in increased WSI_{ag} in nearly a quarter of total croplands, mostly in North America, Europe, and Southern China. The ET_c is largely contributed by the four major crops, that is, wheat, rice, maize, and soybeans, during the months under water scarcity (see Figure S3 in Supporting Information S1). Besides the four crops, barley and cotton also contribute the largest ET_c in most of their major production region. The changes in WA will be dominated by WA_{green} in ∼16% of total croplands, including the regions where increased WA dominated the ΔWSI_{ag} and a few regions in North America, Europe, and Southern Africa where decreased WA dominated.

4. Discussion

4.1. Difference Between WSI$_{ag}$ and Other Agricultural Water Scarcity Indices

The WSI$_{ag}$ is an integrated index, using the same concept as that of W. Liu et al. (2022), was initially designed to incorporate blue and green water availability so that it is applicable to both irrigated and rainfed croplands. It is expected to overcome the deficiency of the traditional water scarcity index, that is, the ratio of water withdrawal to water availability, which cannot represent the agricultural water stress in rainfed cropland because of no withdrawal for irrigation. The major difference between W. Liu et al. (2022) and our study is that the former focused on the comparison between the new WSI$_{ag}$ and the traditional water scarcity index, while we focused on the spatially explicit assessment of agricultural water scarcity under future climate change and identification of the major contributing factors to the changes in, especially intensified, water scarcity in the future. It should also be noted that we used improved methods for the calculations of crop requirements (ET$_c$) and green water availability, which are important to more accurately assess the agriculture related water scarcity. By using the methods in this study, we could obtain more reasonable estimates of ET$_c$ based on ET0 and relatively more accurate estimates of green water availability given by the PCR-GLOBWB model in most cases.

It was reported that ∼80% or more of the global crop water consumption was provided by green water (J. Liu & Yang, 2010; Mekonnen & Hoekstra, 2011). The global green water use was estimated at 6,891 km^3/year in this study, while it ranges from 4,886 to 7,670 km^3/year provided by the selected previous studies (Table S6 in Supporting Information S1). The global blue WA was estimated at 49,871 km^3/year for during 1971–2000, which compares well with the multimodel results that ranges from 42,000 to 66,000 km^3/year during 1985–1999 (Haddeland et al., 2011). This study also differs from Rosa et al. (2020) that mainly focused on the situation when there was green water scarcity but no blue water scarcity. In a sense, the green water scarcity can be better represented by using a green water scarcity index (e.g., Veettil & Mishra, 2020). However, it is worthy of note that using a green water scarcity index alone cannot identify the situation with green water stress but without blue water stress. This is well addressed by the integrated index WSI$_{ag}$, which can detect water stress in both rainfed and irrigated croplands either caused by green water deficit or blue water shortage. Thus, the WSI$_{ag}$ could be an effective tool for the monitoring or assessment of agricultural water scarcity.

4.2. Intensified Agricultural Water Scarcity in Warming and Drier Climate

The WSI$_{ag}$ would be intensified worldwide in the future, which is largely affected by changes in ET$_c$ and WA. ET$_c$ would increase prevalently over the world due to global warming in the future. In contrast to ET$_c$, future changes in WA vary largely over regions. WA$_{blue}$ and WA$_{green}$ show opposite changes in some areas due to the different patterns of the future changes in temperature and precipitation. For example, in East Asia, more precipitation will increase WA$_{green}$ but not necessarily increase WA$_{blue}$ because the prevalent warming will increase ET and reduce runoff. Different changing patterns in WA between the two scenarios were also found in Amazonia, Southern Africa, and Central Asia, the regions with different warming levels and precipitation changes.

Overall, changes in WA will dominate the changes in WSI$_{ag}$ in three fourths of total croplands while changes in ET$_c$ will dominate in nearly a quarter of total croplands. By increasing ET$_c$, global warming would intensify agriculture water scarcity in considerable regions of North America and Europe. In addition, both warming and decreased precipitation would result in less WA, which would increase WSI$_{ag}$ in ∼60% of total croplands. WA$_{green}$ dominates the changes in WA in some regions with chronic water scarcity (e.g., North China and North India where irrigation heavily relied on groundwater pumping), which suggested the necessity of including WA$_{green}$ in agricultural water scarcity assessment and that it could not be overlooked in agricultural water management in those regions.

4.3. Regional and Seasonal Features of Future Agricultural Water Scarcity

The agricultural water scarcity showed distinct responses to climate change over regions and thus may require different strategies for mitigation. Future agricultural water scarcity would increase in many croplands and arid regions where have experienced water scarcity during the baseline period, and decrease in only a small percentage of croplands. Prevalent water scarcity was mostly found in semiarid/semihumid regions with intensive croplands such as North China, Central America, and Australia, but was also found in India where has the largest

croplands in the world. The seasonal A_{ws} showed distinct patterns between these regions. In the United States and Northern Europe, A_{ws} was large and would increase more in the future during the growing season, while in other regions A_{ws} seemed to be not related to growing seasons. Nevertheless, it is noted that future A_{ws} generally decrease during April–September in North China and increase in other months, while A_{ws} would increase during May–October and decrease in other months in Southern South America. This would have some implications for the agricultural water management to adapt to future climate change, for example, improved regulation of water storage between seasons via reservoirs. Overall, the seasonality of agricultural water scarcity was not only associated with the phenology of crops but also largely affected by the variations of monthly WA. Understanding the seasonality of both of them would be in favor of agricultural water management in these representative regions under future climate change.

4.4. Implications for Crop Production and Possible Adaptation to Climate Change

The increasing extent and intensity of agricultural water scarcity would probably reduce crop production in the future. Global warming would accelerate evaporation from soils and crops (Figure 2), which in combination with the reduction of precipitation would result in severe water scarcity and even significant soil desiccation in some arid regions like the Middle East and Central Asia. In this study, the importance of green water use for agricultural production was reflected in the regions with intensive croplands (e.g., northern China, India, and Central America) or some arid regions (e.g., the South of Sahel). Future projections suggested that green water availability might increase in northern China and the South of Sahel and thus alleviate agricultural water scarcity, but might further decrease in North India and Central America and thus aggravate water scarcity and put a serious threat to food production. Improvement of green water management could not only directly modulate the agricultural water scarcity but might also regulate blue water availability since the blue and green water can be transferred to each other. Consideration of the seasonality of both blue and green water would help adjust crop structure to adapt to climate change and mitigate the impacts of climate-induced water scarcity.

The largest ET_c is projected to be produced by the major crops (wheat, rice, maize, and soybean, barley, and cotton) globally. Considering the key role of the major crops in global food security, it is unlikely to reduce these croplands globally to decrease the A_{ws}. Rotational fallowing of croplands might largely reduce water scarcity risks and improve the sustainability of agro-ecosystem (Richter et al., 2020), which, however, may also reduce crop production and may not be the first choice in the regions where there would be starvation (FAO, 2018). Increasing crop yield and reducing water consumption in crop production would be an urgent need in view of the relatively low irrigation efficiency in the countries with large croplands (e.g., China and India) in the context of the increasing global food demands and the globally intensified agricultural water scarcity. Improving irrigation infrastructure and efficiency is one of the key ways to reduce crop water consumption and alleviate the risks of agricultural water scarcity. Blue water availability for agricultural irrigation could be extended by reallocating water resources within basins (Z. Huang et al., 2021) and more efficiently used by increasing IE (Equation 2). On the other hand, agricultural water scarcity in both irrigated and rainfed croplands might be mitigated if green water can be fully and more efficiently utilized, for example, reducing evaporation from bare soil (Dlamini et al., 2017). Developing climate adaptation strategies with consideration of green water use and availability is critical for reducing the impacts of intensified water scarcity toward food security and sustainable agro-ecosystem in the coming decades.

4.5. Limitations in the Estimates of Agricultural Water Scarcity

The WSI_{ag} involves several key processes of hydrology, crops, and human activities, it was then subject to uncertainties in the estimates related to these processes. For example, the relative large grid cell size overlooks the variabilities of the blue and green water within cropland (Veettil et al., 2022), the national IE cannot represent the variation of irrigation efficiency across regions, these limitation may lessen the implication of the findings at local scale. Future changes in cropland have direct impacts on the estimates of ET_c whereas the change in green water was sensitive to the changes in land use pattern (Z. Huang et al., 2019; X. Liu et al., 2017; Veettil & Mishra, 2018). In this study, present (the year 2005) croplands were used for the future projections and the potential impacts of cropland change were not reflected. The trajectory of the future socioeconomic conditions was also not considered. The use of present conditions may result in an underestimation of agricultural water scarcity in the future. Nevertheless, the projections of WSI_{ag} based on the present croplands can still be a reference assessment that quantifies the impacts of climate change on agricultural water scarcity.

Groundwater, desalination water, and recycled water were not considered in the estimation of WA_{blue}. This may cause an overestimation of WA, consequently WSI_{ag}. Groundwater pumping is an important water resource for agricultural irrigation in many regions of the world, for example, North China (Cao et al., 2013) and Northwest India (Rodell et al., 2018). In wet regions, the blue and green water availability may not be underestimated too much because consumption of groundwater would be recharged by river flow or soil moisture. However, WA_{blue} could be underestimated in dry regions where groundwater is a major source of irrigation. The simulations of groundwater were subject to considerable uncertainty at the global scale (Wada, 2016), which makes it challenging to include groundwater availability in WA_{blue}. It should be noted that degradation of water quality under future climate change (W. Liu et al., 2020) has adverse impacts such as decreasing WA_{blue} (van Vliet et al., 2017). Without consideration of water quality would result in overestimation of WA and thus underestimation of WSI_{ag} (W. Liu et al., 2019).

The calculation of EFR worldwide was also subject to large uncertainties (X. Liu et al., 2021). There were several EFR estimation methods, which may provide various EFR estimates (Pastor et al., 2014). EFR would also be significantly different for ecological conservation goals across regions. Richter et al. (2012) suggested that 80% of daily flow would maintain ecological integrity in most rivers, and 90% may be needed to protect rivers with at-risk species. The EFR suggested by the Tennant method can range from 10% to more than 100% of mean annual flow in different seasons for different ecological statuses (Tennant, 1976). For simplicity, only one method (VMF) was used in this study, which was designed to reflect the natural variability of streamflow and to be applicable in most rivers in the Anthropocene (Pastor et al., 2014).

This assessment considered 19 major crops which cover nearly 80% of the global total croplands. A full consideration of all crops would further narrow the uncertainty in the assessment and provide more comprehensive insights into the agricultural water scarcity in all regions of the world.

Finally, the WSI assessment in this study was based on the projections from the hydrological model, PCR-GLOBWB, forced by four GCMs. Large uncertainties were expected in the future projections. However, our study focuses on building an WSI_{ag} that explicitly incorporates green water in the assessment. We acknowledge that uncertainties in the input data could affect the estimated WSIs values across regions, but an improvement in the accuracy of input data is beyond the scope of this study.

5. Conclusions

Global agricultural water scarcity in the past (1981–2005) and in the near future (2026–2050) is estimated by using an index (WSI_{ag}) incorporating both blue water, green water resources, and EFRs. The future WSI_{ag} was calculated based on the projections of two global hydrological models and four global climate models under the RCP2.6 and RCP6.0 scenarios. The results suggested that ∼3.8 million km^2 croplands, accounting for ∼39% of global total croplands would experience water scarcity in the future under both scenarios, which was ∼3% more than the baseline period. In the future, the degree of agricultural water scarcity would increase in 83%–84% of total croplands, for example, in Central and Eastern United States, Amazonia, Northern Europe, Southern Africa, and North India. The intensified water scarcity would be dominated by the decreasing water availability in ∼60% of total croplands and by increasing crop water requirements in nearly a quarter of croplands. The significant contribution of the changes in green water availability (in ∼16% of total croplands) to WSI_{ag} indicated its important role in agricultural water scarcity assessment, particularly in the regions with dense croplands. This study highlighted the necessity of including green water availability in agricultural water scarcity assessment and future agricultural water management toward mitigation of climate change. The findings would enhance our understanding of water scarcity and the necessity of improving the utilization of green water in croplands that may alleviate water scarcity in a warming climate in the future.

Data Availability Statement

The data used in the study are publicly available from https://esg.pik-potsdam.de/projects/isimip/. Data sets for this research are available at https://doi.org/10.5281/zenodo.6332492.

References

Allen, R. G., Pereira, L. S., Raes, D., & Smith, M. (1998). *Crop evapotranspiration—Guidelines for computing crop water requirements*.

Cao, G., Zheng, C., Scanlon, B. R., Liu, J., & Li, W. (2013). Use of flow modeling to assess sustainability of groundwater resources in the North China Plain. *Water Resources Research*, *49*, 159–175. https://doi.org/10.1029/2012WR011899

Dlamini, P., Ukoh, I. B., van Rensburg, L. D., & du Preez, C. C. (2017). Reduction of evaporation from bare soil using plastic and gravel mulches and assessment of gravel mulch for partitioning evapotranspiration under irrigated canola. *Soil Research*, *55*(3), 222–233. https://doi.org/10.1071/SR16098

Dudgeon, D. (2010). Prospects for sustaining freshwater biodiversity in the 21st century: Linking ecosystem structure and function. *Current Opinion in Environmental Sustainability*, *2*(5), 422–430. https://doi.org/10.1016/j.cosust.2010.09.001

FAO. (2018). *The future of food and agriculture—Alternative pathways to 2050* (p. 224). Rome: Food and Agriculture Organization of the United Nations.

Frieler, K., Lange, S., Piontek, F., Reyer, C. P. O., Schewe, J., Warszawski, L., et al. (2017). Assessing the impacts of 1.5°C global warming—Simulation protocol of the Inter-Sectoral Impact Model Intercomparison Project (ISIMIP2b). *Geoscientific Model Development*, *10*(12), 4321–4345. https://doi.org/10.5194/gmd-10-4321-2017

Gerten, D., Heck, V., Jägermeyr, J., Bodirsky, B. L., Fetzer, I., Jalava, M., et al. (2020). Feeding ten billion people is possible within four terrestrial planetary boundaries. *Nature Sustainability*, *3*(3), 200–208. https://doi.org/10.1038/s41893-019-0465-1

Gerten, D., Heinke, J., Hoff, H., Biemans, H., Fader, M., & Waha, K. (2011). Global water availability and requirements for future food production. *Journal of Hydrometeorology*, *12*(5), 885–899. https://doi.org/10.1175/2011jhm1328.1

Goldewijk, K. K., Beusen, A., Doelman, J., & Stehfest, E. (2017). Anthropogenic land use estimates for the Holocene—HYDE 3.2. *Earth System Science Data*, *9*(2), 927–953. https://doi.org/10.5194/essd-9-927-2017

Haddeland, I., Clark, D. B., Franssen, W., Ludwig, F., Voß, F., Arnell, N. W., et al. (2011). Multimodel estimate of the global terrestrial water balance: Setup and first results. *Journal of Hydrometeorology*, *12*(5), 869–884. https://doi.org/10.1175/2011JHM1324.1

Hanasaki, N., Yoshikawa, S., Pokhrel, Y., & Kanae, S. (2018). A quantitative investigation of the thresholds for two conventional water scarcity indicators using a state-of-the-art global hydrological model with human activities. *Water Resources Research*, *54*, 8279–8294. https://doi.org/10.1029/2018WR022931

Hoekstra, A. Y. (2014). Water scarcity challenges to business. *Nature Climate Change*, *4*(5), 318–320. https://doi.org/10.1038/nclimate2214

Hoekstra, A. Y., Mekonnen, M. M., Chapagain, A. K., Mathews, R. E., & Richter, B. D. (2012). Global monthly water scarcity: Blue water footprints versus blue water availability. *PLoS One*, *7*(2), e32688. https://doi.org/10.1371/journal.pone.0032688

Huang, J., Yu, H., Dai, A., Wei, Y., & Kang, L. (2017). Drylands face potential threat under 2°C global warming target. *Nature Climate Change*, *7*(6), 417–422. https://doi.org/10.1038/nclimate3275

Huang, Z., Hejazi, M., Tang, Q., Vernon, C. R., Liu, Y., Chen, M., & Calvin, K. (2019). Global agricultural green and blue water consumption under future climate and land use changes. *Journal of Hydrology*, *574*, 242–256. https://doi.org/10.1016/j.jhydrol.2019.04.046

Huang, Z., Liu, X., Sun, S., Tang, Y., Yuan, X., & Tang, Q. (2021). Global assessment of future sectoral water scarcity under adaptive inner-basin water allocation measures. *The Science of the Total Environment*, *783*, 146973. https://doi.org/10.1016/j.scitotenv.2021.146973

Jägermeyr, J., Pastor, A., Biemans, H., & Gerten, D. (2017). Reconciling irrigated food production with environmental flows for Sustainable Development Goals implementation. *Nature Communications*, *8*(1), 1–9. https://doi.org/10.1038/ncomms15900

Liu, J., & Yang, H. (2010). Spatially explicit assessment of global consumptive water uses in cropland: Green and blue water. *Journal of Hydrology*, *384*(3), 187–197. https://doi.org/10.1016/j.jhydrol.2009.11.024

Liu, J., Yang, H., Gosling, S. N., Kummu, M., Flörke, M., Pfister, S., et al. (2017). Water scarcity assessments in the past, present, and future. *Earth's Future*, *5*, 545–559. https://doi.org/10.1002/2016EF000518

Liu, W., Antonelli, M., Kummu, M., Zhao, X., Wu, P., Liu, J., et al. (2019). Savings and losses of global water resources in food-related virtual water trade. *Wiley Interdisciplinary Reviews: Water*, *6*(1), e1320. https://doi.org/10.1002/wat2.1320

Liu, W., Ciais, P., Liu, X., Yang, H., Hoekstra, A. Y., Tang, Q., et al. (2020). Global phosphorus losses from croplands under future precipitation scenarios. *Environmental Science & Technology*, *54*, 14761–14771. https://doi.org/10.1021/acs.est.0c03978

Liu, W., Liu, X., Yang, H., Ciais, P., & Wada, Y. (2022). Global water scarcity assessment incorporating green water in crop production. *Water Resources Research*, *58*, e2020WR028570. https://doi.org/10.1029/2020WR028570

Liu, X., Liu, W., Liu, L., Tang, Q., Liu, J., & Yang, H. (2021). Environmental flow requirements largely reshape global surface water scarcity assessment. *Environmental Research Letters*, *16*(10), 104029. https://doi.org/10.1088/1748-9326/ac27cb

Liu, X., Tang, Q., Cui, H., Mengfei, M., Gerten, D., Gosling, S., et al. (2017). Multimodel uncertainty changes in simulated river flows induced by human impact parameterizations. *Environmental Research Letters*, *12*(2), 025009. https://doi.org/10.1088/1748-9326/aa5a3a

Liu, X., Tang, Q., Liu, W., Veldkamp, T. I. E., Boulange, J., Liu, J., et al. (2019). A spatially explicit assessment of growing water stress in China from the past to the future. *Earth's Future*, *7*, 1027–1043. https://doi.org/10.1029/2019EF001181

Mekonnen, M. M., & Hoekstra, A. Y. (2011). The green, blue and grey water footprint of crops and derived crop products. *Hydrology and Earth System Sciences*, *15*(5), 1577–1600. https://doi.org/10.5194/hess-15-1577-2011

Núñez, M., Pfister, S., Roux, P., & Antón, A. (2013). Estimating water consumption of potential natural vegetation on global dry lands: Building an LCA framework for green water flows. *Environmental Science & Technology*, *47*(21), 12258–12265. https://doi.org/10.1021/es403159t

Oki, T., & Kanae, S. (2006). Global hydrological cycles and world water resources. *Science*, *313*(5790), 1068–1072. https://doi.org/10.1126/science.1128845

Pastor, A. V., Ludwig, F., Biemans, H., Hoff, H., & Kabat, P. (2014). Accounting for environmental flow requirements in global water assessments. *Hydrology and Earth System Sciences*, *18*(12), 5041–5059. https://doi.org/10.5194/hess-18-5041-2014

Pastor, A. V., Palazzo, A., Havlik, P., Biemans, H., Wada, Y., Obersteiner, M., et al. (2019). The global nexus of food–trade–water sustaining environmental flows by 2050. *Nature Sustainability*, *2*(6), 499–507. https://doi.org/10.1038/s41893-019-0287-1

Portmann, F. T., Siebert, S., & Döll, P. (2010). MIRCA2000—Global monthly irrigated and rainfed crop areas around the year 2000: A new high-resolution data set for agricultural and hydrological modeling. *Global Biogeochemical Cycles*, *24*, GB1011. https://doi.org/10.1029/2008GB003435

Quinteiro, P., Rafael, S., Vicente, B., Marta-Almeida, M., Rocha, A., Arroja, L., & Dias, A. C. (2019). Mapping green water scarcity under climate change: A case study of Portugal. *The Science of the Total Environment*, *696*, 134024. https://doi.org/10.1016/j.scitotenv.2019.134024

Quinteiro, P., Rafael, S., Villanueva-Rey, P., Ridoutt, B., Lopes, M., Arroja, L., & Dias, A. C. (2018). A characterisation model to address the environmental impact of green water flows for water scarcity footprints. *The Science of the Total Environment*, *626*, 1210–1218. https://doi.org/10.1016/j.scitotenv.2018.01.201

Richter, B. D., Bartak, D., Caldwell, P., Davis, K. F., Debaere, P., Hoekstra, A. Y., et al. (2020). Water scarcity and fish imperilment driven by beef production. *Nature Sustainability*, *3*(4), 319–328. https://doi.org/10.1038/s41893-020-0483-z

Richter, B. D., Davis, M. M., Apse, C., & Konrad, C. (2012). A presumptive standard for environmental flow protection. *River Research and Applications*, *28*(8), 1312–1321. https://doi.org/10.1002/rra.1511

Rodell, M., Famiglietti, J. S., Wiese, D. N., Reager, J. T., Beaudoing, H. K., Landerer, F. W., & Lo, M. H. (2018). Emerging trends in global freshwater availability. *Nature*, *557*(7707), 651–659. https://doi.org/10.1038/s41586-018-0123-1

Rodrigues, D. B. B., Gupta, H. V., & Mendiondo, E. M. (2014). A blue/green water-based accounting framework for assessment of water security. *Water Resources Research*, *50*, 7187–7205. https://doi.org/10.1002/2013WR014274

Rohwer, J., Gerten, D., & Lucht, W. (2007). *Development of functional irrigation types for improved global crop modelling*. Potsdam: PIK.

Rosa, L., Chiarelli, D. D., Rulli, M. C., Dell'Angelo, J., & D'Odorico, P. (2020). Global agricultural economic water scarcity. *Science Advances*, *6*(18), eaaz6031. https://doi.org/10.1126/sciadv.aaz6031

Schewe, J., Heinke, J., Gerten, D., Haddeland, I., Arnell, N. W., Clark, D. B., et al. (2014). Multimodel assessment of water scarcity under climate change. *Proceedings of the National Academy of Sciences of the United States of America*, *111*(9), 3245–3250. https://doi.org/10.1073/pnas.1222460110

Schyns, J. F., Hoekstra, A. Y., Booij, M. J., Hogeboom, R. J., & Mekonnen, M. M. (2019). Limits to the world's green water resources for food, feed, fiber, timber, and bioenergy. *Proceedings of the National Academy of Sciences of the United States of America*, *116*(11), 4893–4898. https://doi.org/10.1073/pnas.1817380116

Sheffield, J., Goteti, G., & Wood, E. F. (2006). Development of a 50-year high-resolution global dataset of meteorological forcings for land surface modeling. *Journal of Climate*, *19*(13), 3088–3111. https://doi.org/10.1175/jcli3790.1

Tang, Q. (2020). Global change hydrology: Terrestrial water cycle and global change. *Science China Earth Sciences*, *63*, 459–462. https://doi.org/10.1007/s11430-019-9559-9

Tennant, D. L. (1976). Instream flow regimens for fish, wildlife, recreation and related environmental resources. *Fisheries*, *1*(4), 6–10. https://doi.org/10.1577/1548-8446(1976)001<0006:IFRFFW>2.0.CO;2;2

Tong, S., Berry, H. L., Ebi, K., Bambrick, H., Hu, W., Green, D., et al. (2016). Climate change, food, water and population health in China. *Bulletin of the World Health Organization*, *94*(10), 759–765. https://doi.org/10.2471/blt.15.167031

van Vliet, M. T. H., Flörke, M., & Wada, Y. (2017). Quality matters for water scarcity. *Nature Geoscience*, *10*, 800–802. https://doi.org/10.1038/ngeo3047

Veettil, A. V., & Mishra, A. K. (2016). Water security assessment using blue and green water footprint concepts. *Journal of Hydrology*, *542*, 589–602. https://doi.org/10.1016/j.jhydrol.2016.09.032

Veettil, A. V., & Mishra, A. K. (2018). Potential influence of climate and anthropogenic variables on water security using blue and green water scarcity, Falkenmark index, and freshwater provision indicator. *Journal of Environmental Management*, *228*, 346–362. https://doi.org/10.1016/j.jenvman.2018.09.012

Veettil, A. V., & Mishra, A. (2020). Water security assessment for the Contiguous United States using water footprint concepts. *Geophysical Research Letters*, *47*, e2020GL087061. https://doi.org/10.1029/2020GL087061

Veettil, A. V., Mishra, A. K., & Green, T. R. (2022). Explaining water security indicators using hydrologic and agricultural systems models. *Journal of Hydrology*, *607*, 127463. https://doi.org/10.1016/j.jhydrol.2022.127463

Vörösmarty, C. J., Green, P., Salisbury, J., & Lammers, R. B. (2000). Global water resources: Vulnerability from climate change and population growth. *Science*, *289*(5477), 284–288. https://doi.org/10.1126/science.289.5477.284

Wada, Y. (2016). Modeling groundwater depletion at regional and global scales: Present state and future prospects. *Surveys in Geophysics*, *37*(2), 419–451. https://doi.org/10.1007/s10712-015-9347-x

Wada, Y., Flörke, M., Hanasaki, N., Eisner, S., Fischer, G., Tramberend, S., et al. (2016). Modeling global water use for the 21st century: The Water Futures and Solutions (WFaS) initiative and its approaches. *Geoscientific Model Development*, *9*(1), 175–222. https://doi.org/10.5194/gmd-9-175-2016

Wada, Y., van Beek, L. P. H., Viviroli, D., Dürr, H. H., Weingartner, R., & Bierkens, M. F. P. (2011). Global monthly water stress: 2. Water demand and severity of water stress. *Water Resources Research*, *47*, W07518. https://doi.org/10.1029/2010WR009792

Wada, Y., Wisser, D., & Bierkens, M. F. P. (2014). Global modeling of withdrawal, allocation and consumptive use of surface water and groundwater resources. *Earth System Dynamics*, *5*(1), 15–40. https://doi.org/10.5194/esd-5-15-2014

Ward, F. A., & Pulido-Velazquez, M. (2008). Water conservation in irrigation can increase water use. *Proceedings of the National Academy of Sciences of the United States of America*, *105*(47), 18215–18220. https://doi.org/10.1073/pnas.0805554105

Weedon, G. P., Balsamo, G., Bellouin, N., Gomes, S., Best, M. J., & Viterbo, P. (2014). The WFDEI meteorological forcing data set: WATCH forcing data methodology applied to ERA-Interim reanalysis data. *Water Resources Research*, *50*, 7505–7514. https://doi.org/10.1002/2014WR015638

Yin, Y., Tang, Q., Liu, X., & Zhang, X. (2017). Water scarcity under various socio-economic pathways and its potential effects on food production in the Yellow River basin. *Hydrology and Earth System Sciences*, *21*(2), 791–804. https://doi.org/10.5194/hess-21-791-2017